Crack formation in the tungsten armour of divertor targets under high heat flux loads: A computational fracture mechanics study

Kuo Zhang[1,2], Jeong-Ha You[1]

1. Max Planck Institute of Plasma Physics, Boltzmannstraße 2, 85748 Garching, Germany
2. Karlsruhe Institute of Technology, Institute for Applied Materials, Hermann-von-Helmholtz-Platz 1, 76344 Eggenstein-Leopoldshafen, Germany

Abstract

In the framework of EUROfusion, the thermally induced stress and the consequential fracture of the design of DEMO-divertor with copper alloy heat sink have been analyzed, to assess the structural integrity of tungsten armor of the plasma facing component (PFC). With finite element method (FEM), the influence of mesh and plasticity of tungsten has been evaluated. Due to the lack of material data, especially those of irradiated tungsten under operation conditions, conservative assumptions have been made in terms of plasticity, fracture strength and fracture toughness. The crack initiation and propagation with assumed plasticity and fracture toughness for heat fluxes ranging from 10MW/m^2 up to 30 MW/m^2 have been analyzed. Thermal stress analysis has been performed with various plasticity of tungsten, to locate the peak stress, which leads to the highest possibility of crack initiation. Extended finite element method (XFEM) analysis has been performed afterwards with various fracture strength toughness. The influence of plasticity and fracture toughness from almost zero up to K_{ic} = 20MPa·m$^{1/2}$ has been evaluated. The predicted crack propagation has been verified by results of J-integral calculation.

Abbreviation

FEM	Finite element method
PFC	Plasma facing component
XFEM	Extended finite element method
HRP	Hot radial pressing
MPH	Material properties handbook
DBTT	Ductile-to-brittle-transition-temperature

1. Introduction

In the work package WP-DIV of EUROfusion for European DEMO, robust divertor designs are required [1] to meet the crucial prerequisites for reliable power handling of a commercially viable fusion power plant as described in the European Fusion Roadmap to electricity [2, 3]. Due to the complicated working conditions in a fusion reactor, the components are expected to experience combined extreme thermal, mechanical and physical impact [1, 2].

Beside the lack of material data, especially the irradiation test data with high damage dose in DEMO, full characterizations of the related materials and full experimental verification of lifetime is virtually not possible for the real working condition. Hence, the research for the design follows the concept of "design-by-analysis" [4] with conservative assumptions of plasticity, fracture strength and fracture toughness. The work aims to locate the potential weak points in the design where cracks most likely initiate, and to estimate how far the crack will propagate.

In this article, a series of FEM simulations are presented and discussed, using various assumptions on plasticity model as well as fracture strength and toughness data. The capability as well as issues about the FEM simulation with ABAQUS are discussed.

2. Dimension and boundary conditions

The dimension of a divertor design option as used in WPDIV is 23×28×12 mm^3 (Figure 1). The cooling pipe is made of CuCrZr, with thickness of 1.5mm and inner diameter of 12mm. Between the CuCrZr cooling pipe and W, there is a 1mm thick pure Cu interlayer. The shortest distance from the plasma-facing surface to this Cu interlayer is 8 mm. Comparing to the previous design [5], the current design has this 8mm armor thickness instead of 5mm to assure a longer erosion lifetime [6].

The boundary conditions are the same as in the previous research [6], where the coolant temperature is 150°C, hydraulic pressure 5MPa with velocity 16m/s. The heat transfer coefficient also follows the previous values, which has been calculated using Sieder/Tate [7] and CEA/Thom [8] correlations with swirl tape.

The initial stress-released state during fabrication is set to be at temperature 580°C according to hot radial pressing (HRP) process in ENEA [9]. The complete thermal history is included for modelling: The component is cooled from this stress-released state at 580°C to 20°C and then pre-heated to coolant temperature. It is then heated up by heat fluxes for 10 seconds, and cooled by cooling water for another 20 seconds. Such heating-cooling process is repeated for up to 10 cycles.

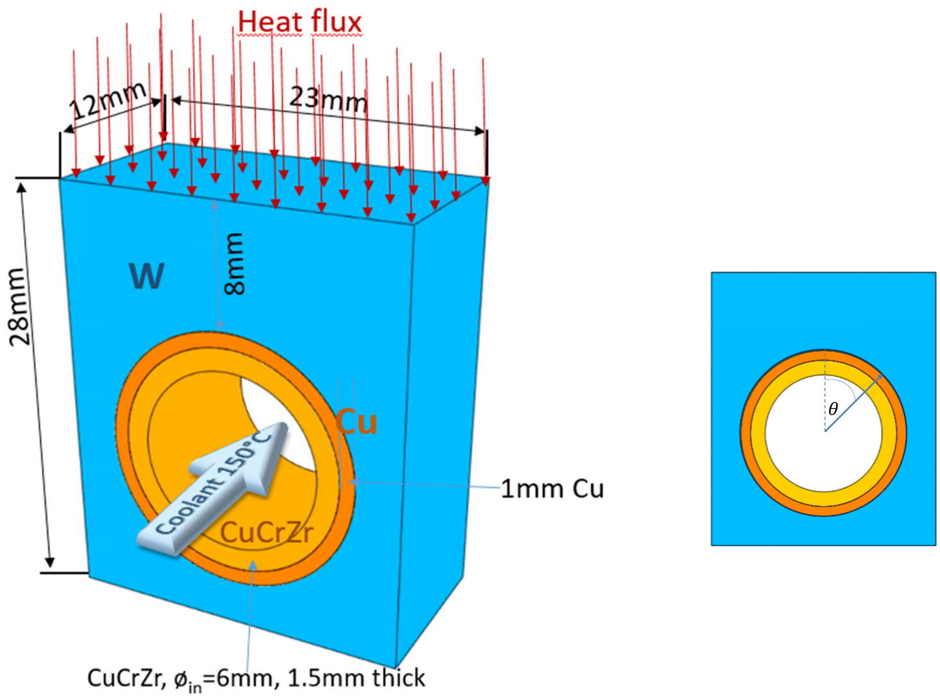

Figure 1 Dimensions and boundary conditions of divertor design option. The origin of cylindrical coordinate system located at the center of CuCrZr-heatsink.

Beside the previous symmetric half or quarter ABAQUS model, also full size models have been built in order to avoid any possible error in setting in the half/quarter model. Three parts constructed by W, Cu and CuCrZr have been built in separate part instances, for more flexibilities in defining the joint in between.

The material data of W, Cu and CuCrZr have generally followed those in the previous research [6], and have been modified according to ITER SDC-IC [10], ITER material properties handbook (MPH) [11] and EUROfusion project internal data base compiled MPH (Material Property Handbooks) [12].

The applied heat fluxes include 10, 15, 20, 25 and 30 MW/m^2. The FEM-calculated temperature profiles under 20MW/m^2 is shown in Figure 2.

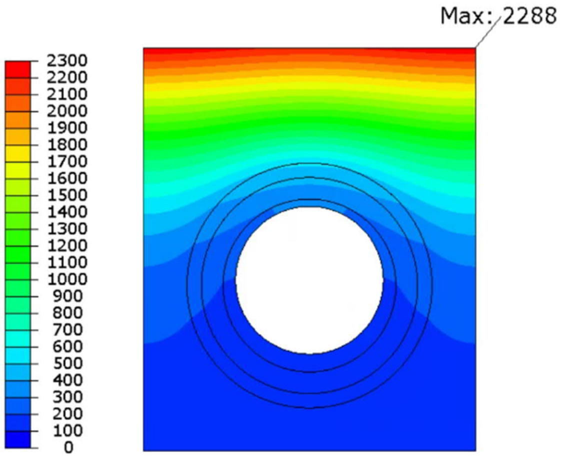

Figure 2 Temperature (°C) profiles of heat fluxes 20MW/m^2

The calculated peak temperatures for these heat fluxes are listed in Table 1.

Heat flux	10 MW/m^2	15 MW/m^2	20 MW/m^2	25 MW/m^2	30 MW/m^2
Peak temperature	1110°C	1699°C	2288°C	2864°C	3443°C

Table 1 Calculated peak temperatures with different heat fluxes.

Note that, since no melting is assumed in the FEM simulation, the peak temperature with 30 MW/m^2 is slightly above the actual melting point 3422°C of tungsten. Also no recrystallization of tungsten has been involved in this study.

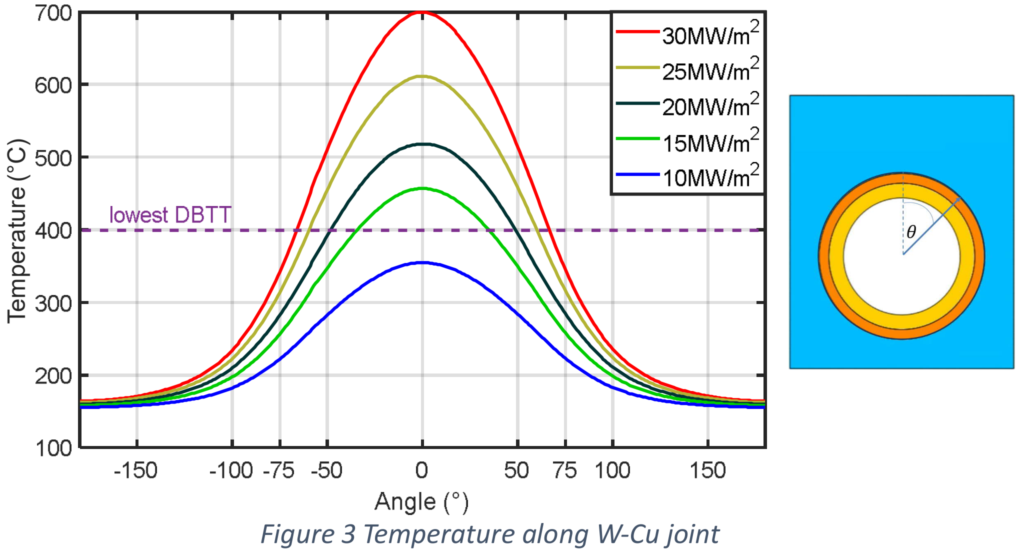

Figure 3 Temperature along W-Cu joint

The temperatures along W-Cu joint versus angle at the end of heating pulse have been collected in Figure 3. Despite the scattered ductile-to-brittle-transition-temperature (DBTT) of tungsten, 400°C is the lowest temperature where the non-linear load displacement behavior on unirradiated tungsten is observed [13] . Still, large region of W-Cu joint has temperate below this DBTT.

3. Analysis of thermally induced stress

In this group of analyses, no crack is considered. The material property of tungsten is either linear-elastic or elastic-ideal plastic.

The aims of these analyses of stress distribution are firstly to find where the cracks most likely initiate, and to evaluate the influence of various factors, including FEM-mesh sensitivity and plasticity.

3.1 Influence of mesh

One of the technical issues is that, the calculated values such as stresses are influenced by the mesh size, shape and element-type in ABAQUS.

Tests have been performed with the average lengths of W-elements' edges close to the W-Cu interface ranging from 0.1mm to 1mm. The calculated peak max. principal stresses in the 1st heating pulse (linear-elastic W) have been collected in Figure 4. The element type applied is linear (C3D8).

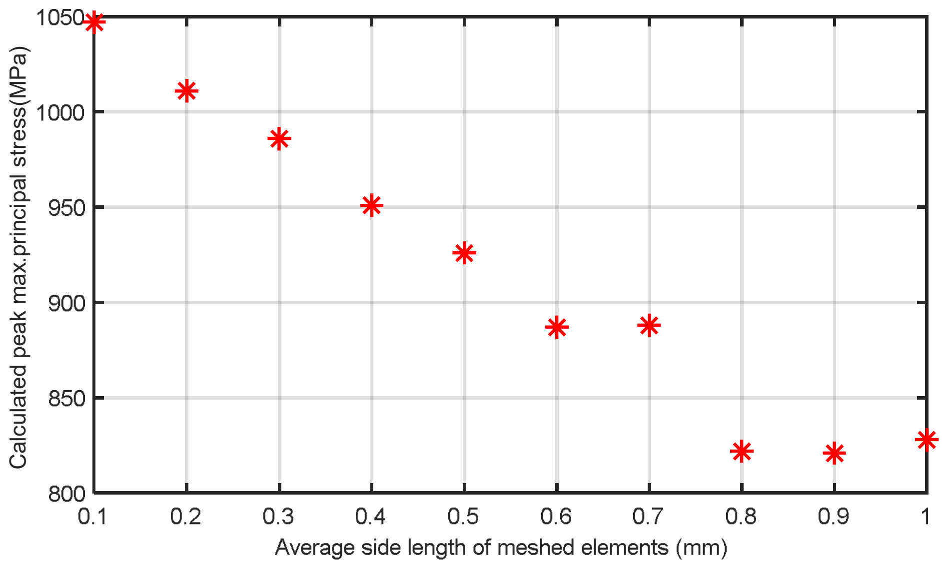

Figure 4 Calculated peak max. principal stress in the 1st heating pulse vs. average length of the element edges in the W block close to the W-Cu interface.

As shown in Figure 4, the calculated peak thermally induced max. principal stresses increase linearly, when the average length of elements' edges decrease from 0.6mm to 0.1mm. Unfortunately, no progressive limit of calculated stress is found by reducing the mesh size with linear element type. On the contrary, the results with 0.8mm, 0.9mm and 1mm as average length of element edge are comparable, which however correspond to coarse mesh.

Quadratic elements show rare dependence on mesh size, since another two simulations have been performed with quadratic elements 1×1×0.6mm^3 and 0.2×0.2×0.6mm^3 as element dimension, the both corresponding peak max. principal stresses are 1164MPa.

Although the results with finer mesh and quadratic element type (C3D20) are principally closer to the reality, however the corresponding increase of meshed elements or quadratic calculation lead to much longer calculation period, especially concerning the difficult convergence in the XFEM calculation for fracture until the 10th heating-cooling cycle, which would be inappropriate and would delay the whole job. Hence linear element type (C3D8) with medium mesh size is applied for the following stress and fracture analysis.

Beside the calculated stresses, the influence of mesh is generally found for the results of XFEM, for instance various meshes lead to different crack initiation locations in XFEM analysis. This is discussed in section 4.3.

3.2 Influence of plasticity

The plasticity of tungsten is found to largely influence the distribution of calculated thermally induced stresses in W-armor.

The plasticity of tungsten is defined to be linear elastic-ideal plastic, and the yield strength is temperature-dependent. The temperature-dependent yield strengths applied in ABAQUS are shown in Figure 5.

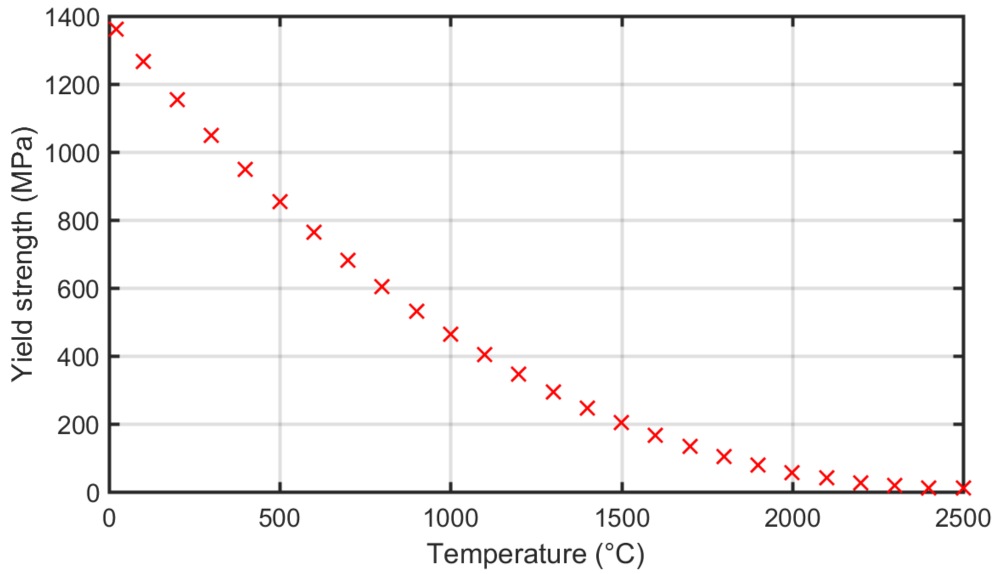

Figure 5 Temperature-dependent yield strength applied in ABAQUS

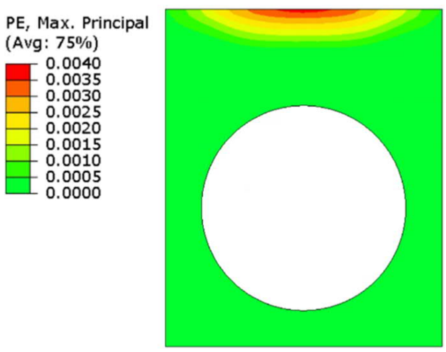

Figure 6 Max.principal plastic strain of elastic-ideal plastic tungsten-armor on the plane of symmetry at the end of heating pulse, heat flux 20MW/m^2.

<table>
<tr><td></td><td>1st pulse</td><td>5th pulse</td></tr>
<tr><td>linear elastic W
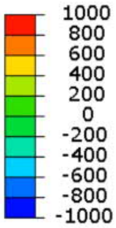</td><td>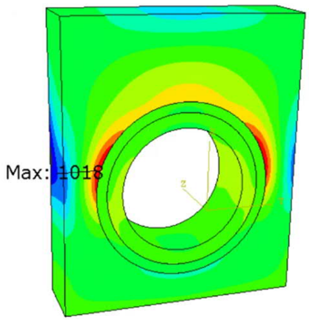
a) Max: 1018MPa</td><td>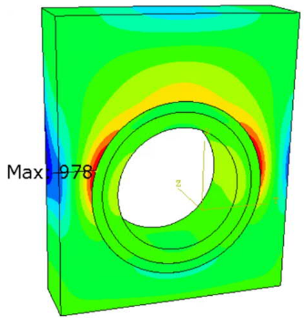
b) Max: 978MPa</td></tr>
<tr><td>elastic-ideal plastic W
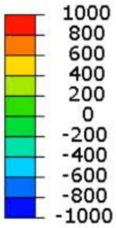</td><td>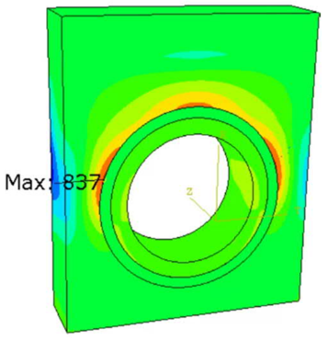
c) Max: 837MPa</td><td>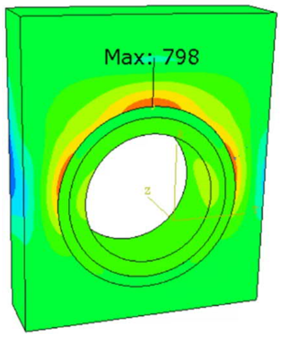
d) Max: 798MPa</td></tr>
</table>

Table 2 Hoop stresses distribution (in cylindrical coordinate system) on the plane of symmetry for a&b) linear elastic W and for c&d) elastic-ideal plastic W, heat flux 20MW/m^2.

Due to the plastic deformation near the plasma-facing surface of tungsten-armor (*Figure 6*), the thermally induced stress within has been changed. Comparing the hoop stresses collected in Table 2, the plasticity of W not only reduces the calculated thermally induced stress, but also causes a jump of the location with the highest hoop stress, from the two sides (around $\pm$75°) to the top position (degree 0)

Similar simulations have also been performed with heat fluxes 10, 15, 25 and 30 MW/m^2. The hoop stresses of W close to W-Cu interface at the end of 1st and 5th heating pulse have been collected and illustrated in Figure 7.

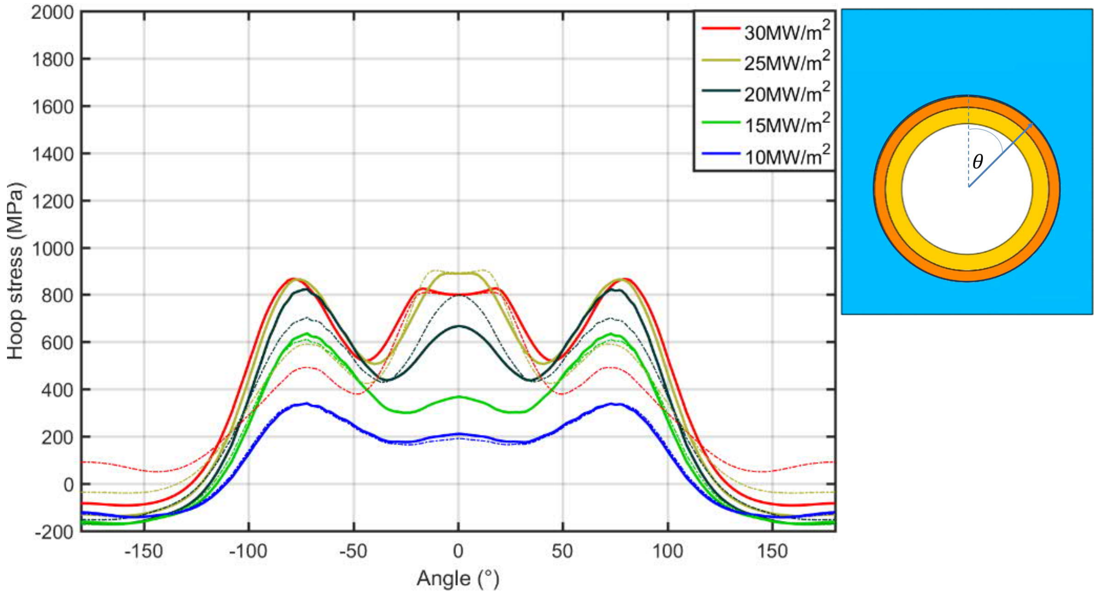

a) elastic-ideal plastic W

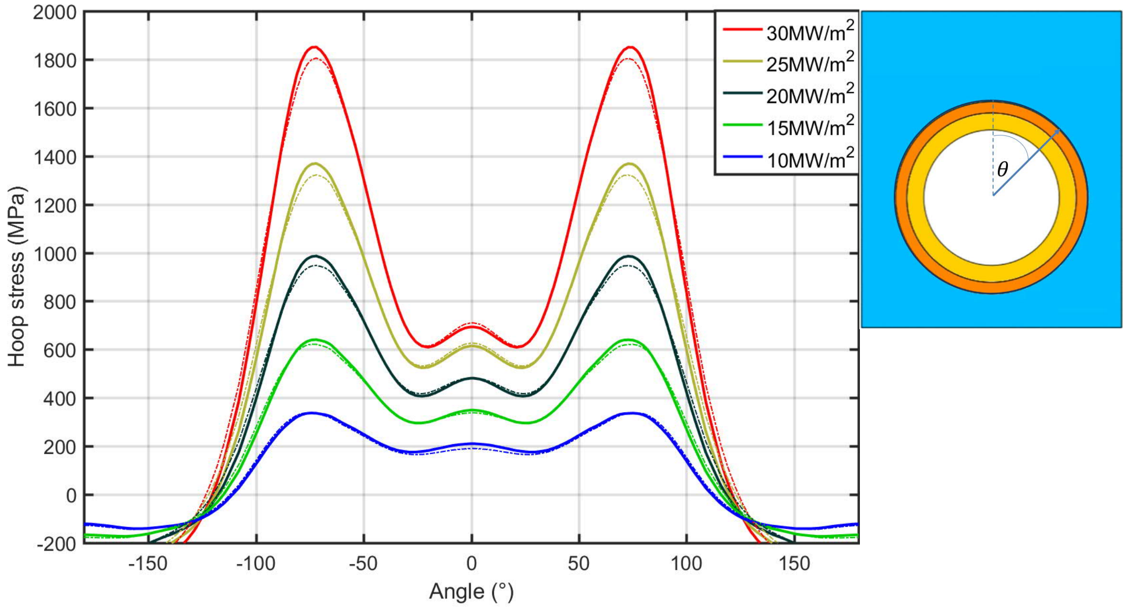

b) Linear elastic W

Figure 7 Hoop stresses of W close to W-Cu interface with a) elastic-ideal plastic W and b) linear elastic W. Solid curves indicate the stress at the end of 1st heating pulse. Dashed curves indicate the stress at the end of 5th heating pulse. The average element size in the W block close to the W-Cu interface is 0.4×0.4×0.5mm^3.

Comparing Figure 7 a) and b), for heat fluxes 10 & 15 MW/m^2, the plasticity of W makes rare difference (0.4% difference for 10 MW/m^2, 2% difference for 15 MW/m^2 on average). For higher heat fluxes, the thermally induced hoop stress is reduced due to the inelastic deformation of W.

In Figure 7 b), for the cases with linear elastic W, the peak hoop stresses always appear at the angle of around degree ±75. However, in Figure 7 a) for the cases with elastic-ideal plastic W, the peak hoop stresses can also appear at the very top (angle zero), for instance at the end of the 5th heating pulse, with heat fluxes 20 & 25 MW/m^2. This is also clear in Table 2 d), by showing the stress profile for heat flux 20MW/m^2.

3.3 Stress analysis with material properties changes

Since the tungsten armor gradually loses its ductility under irradiation, the following simulation has been designed with material property change:

- from the 1st to the 5th heating-cooling cycles, the material property of W in ABAQUS is set to be elastic-ideal plastic.
- Then from the 6th to the 10th heating-cooling cycles, the material property of W is set to be linear elastic since neutron irradiation causes the reduction of ductility of tungsten [14].

Note that this assumption of property change is rare related to the one in operation condition with irradiation in terms of time. Despite the lack of the irradiation test data with high damage dose in DEMO, low irradiation shall need a longer period in order to reduce the ductility of the whole tungsten-armor, and to be pure linear elastic.

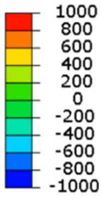 Hoop stresses distribution (in cylindrical coordinate system)	No property change, elastic-ideal plastic W, hoop stress from 6th to 10th heating-cooling cycle	No property change, linear elastic W, hoop stress from 6th to 10th heating-cooling cycle	With material property change: 1st to 5th cycles with elastic-ideal plastic W, 6th to 10th cycles with linear elastic W.
hoop stress at the end of 6th heating pulse	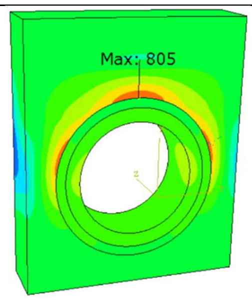 max: 805MPa	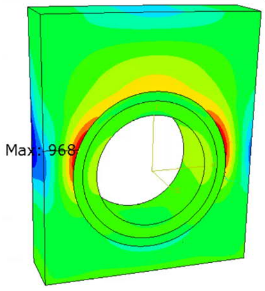 max: 968MPa	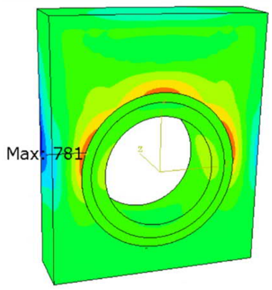 max: 781MPa
hoop stress at the end of 10th heating pulse	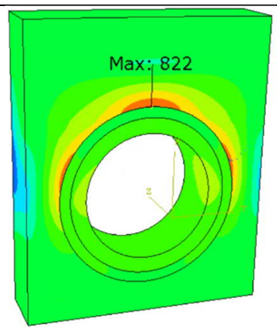 max: 822MPa	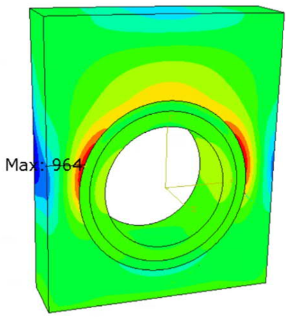 max: 964MPa	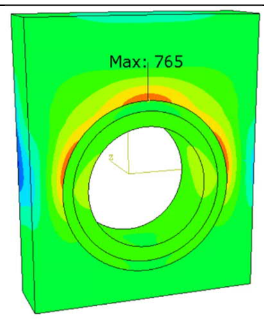 max: 765MPa

Table 3. Hoop stresses distribution (in cylindrical coordinate system) on the plane of symmetry, at the end of heating pulse with heat flux 20MW/m^2. The average element size of W close to W-Cu interface is 0.2×0.2×0.6mm^3

A comparison has been made for heat flux 20MW/m^2 as shown in Table 3.

With material property change, the thermally induced stresses have been largely reduced, comparing to those with always linear elastic W from the 1st to the 10th heating-cooling cycle. The calculated stresses with material property change are also slightly lower than those always with plasticity until the 10th heating-cooling cycle. Hence, this property change not only changes the magnitude of the thermally induced stresses, but also changes the location with peak hoop stress.

Similar simulations have also been performed for heat fluxes 10, 15, 25 and 30 MW/m^2. The hoop stresses of W close to W-Cu interface at the end of 6th and 10th heating pulse have been collected in Figure 8.

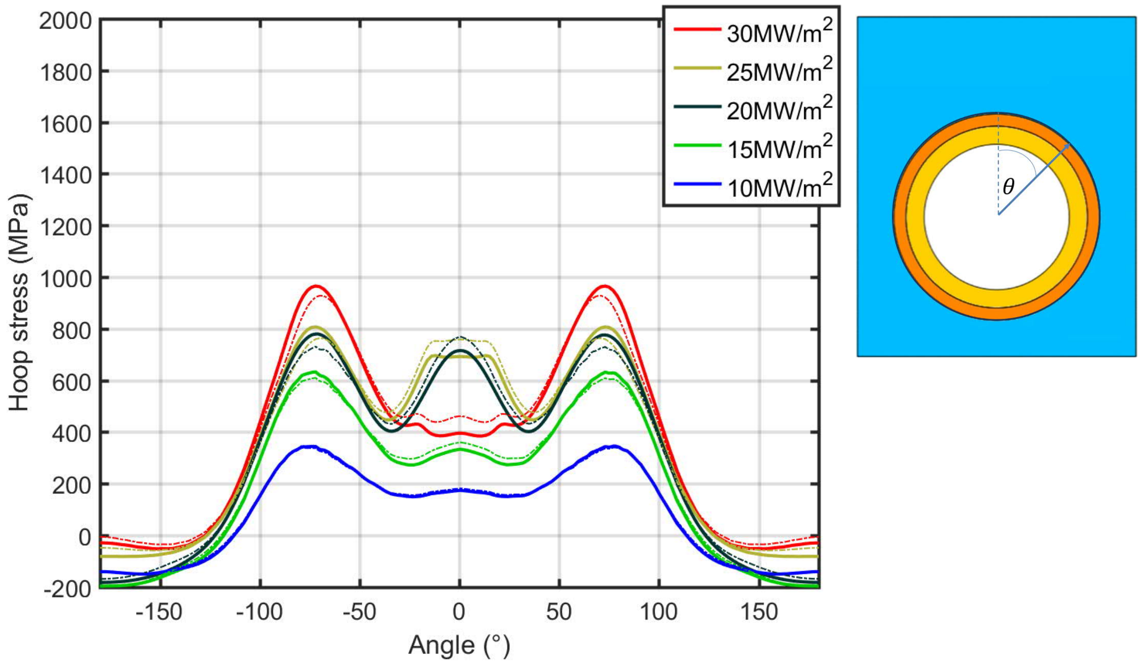

Figure 8. Hoop stresses of W close to W-Cu interface in cylindrical coordinate system on the plane of symmetry with material property changes. Solid curves indicate the stresses at the end of 6th heating pulse. Dashed curves indicate the stresses at the end of 10th heating pulse. The average element size of W close to W-Cu interface is 0.4*0.4*0.5mm^3.

Since the location where peak hoop stress appears has the highest risk of the onset of crack initiation, for heat fluxes 20 MW/m^2, two locations for the crack to initiate are considered: at the very top (angle degree zero) and the two sides (angle ±75°).

For heat fluxes 10 and 15 MW/m^2, the cracks have higher risk to appear at the two sides (angle ±75°).

For heat fluxes 25 and 30 MW/m^2, although peaks at angle ±75° have been found, there are high plastic strains at the top between ±20° , meaning also high probability for crack initiation.

4. Analysis of fracture mechanics

4.1 Simulation of cracks with linear-elastic W

The extended finite element method (XFEM) is a numerical method to study the onset and propagation of cracking in quasi-static problems. XFEM allows you to study crack growth along an arbitrary, solution-dependent path without needing to re-mesh the model [15].

Base on the stress analysis in section 3, XFEM simulations have been performed for various heat fluxes.

This simulation campaign started with linear-elastic W for heat flux 20MW/m^2, with assumed fracture toughness K_{ic} = 2 MPa · $m^{1/2}$ (Critical energy G= K_{ic}^2/E, G = 0.01 mJ/mm^2), fracture strength (max. principal strength) = 500MPa.

This fracture strength 500MPa is chosen as a conservative assumption for tungsten according to data of uniaxial tensile tests of both non-irradiated and irradiated AT&M tungsten up to 1.125 dpa, as reported in [14]. These tensile tests have been performed at 560°C, which is close to the temperature of W close to W-Cu interface at the top (angle 0°) with heat flux 20MW/m^2 as shown in Figure 2 and Figure 3.

Recent test data of neutron-irradiated tungsten (forged ITER grade tungsten produced by Plansee) show that the lower bound of fracture toughness after irradiation up to 1 dpa lies around 5 MPa · $m^{1/2}$, which is regardless of irradiation temperature (see in Figure 9 from [16]). Thus, it is noted that the presently considered toughness value (2 MPa · $m^{1/2}$) is surely a conservative assumption for irradiated tungsten.

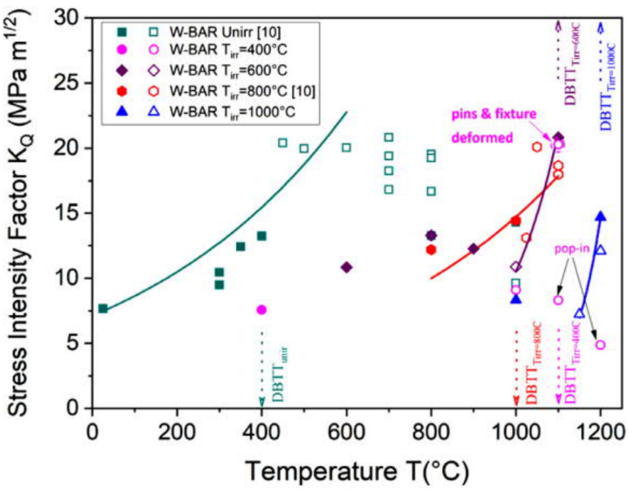

Figure 9 Fracture toughness of the ITER-Grade-Plansee-W bar vs. temperature in the reference unirradiated state and after neutron irradiation to 1 dpa at different temperatures. [16]

The crack (XFEM status) in several steps have been illustrated in Figure 10.

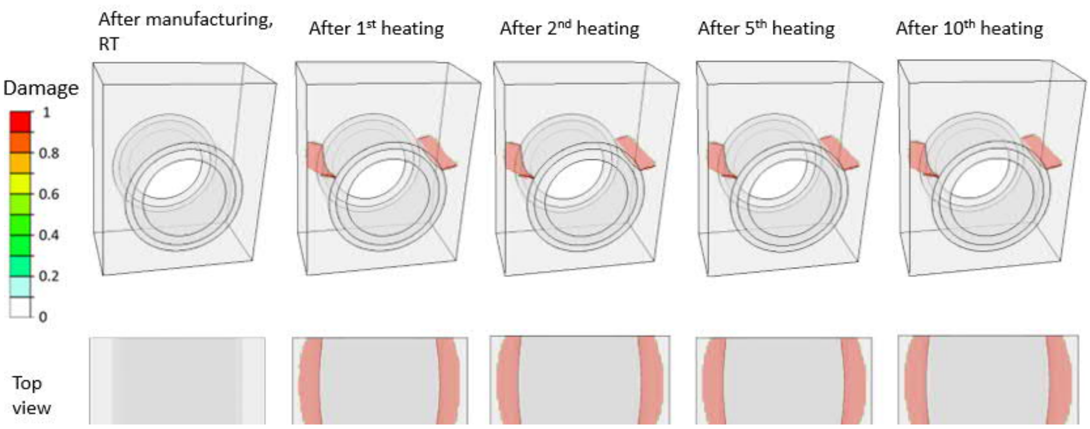

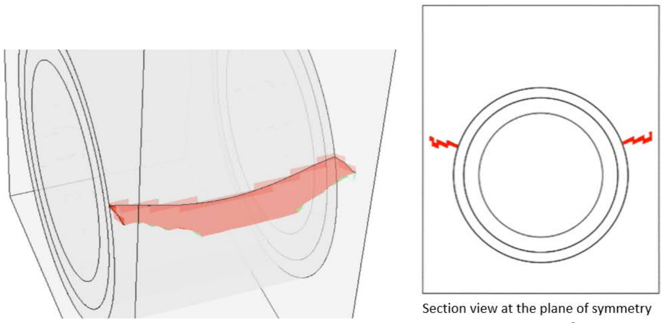

Figure 10 XFEM prediction of crack formation with heat flux 20MW/m^2, critical energy 0.01 mJ/mm^2, linear elastic W, fracture strength (max. principal strength) 500MPa. XFEM status 1 means the crack goes through the element, while XFEM status < 1 means the element is partially cracked. The average element size in the W block close to W-Cu interface is 0.4×0.4×0.5mm^3.

The results shown in Figure 10 indicate that the cracks initiate and propagate in the 1st heating pulse at both sides of angle around ±75°, which agrees with the locations of peak hoop stress shown in Table 2 and the hoop stress distribution shown in Figure 7 b).

The cracks shown in Figure 10 appear in oval and curved shape with peak length on the plane of symmetry.

However, note that there have been also XFEM results where crack only appear on single side, instead of both sides. This happens with different meshes in ABAQUS, although all these meshes are symmetric. Also in the case shown in Figure 10, the cracks on the two sides did not propagate exactly simultaneously, although all factors for asymmetry have been eliminated. It is assumed that "imperfection" have been defined in the default setting of XFEM analysis and some randomized factor has affected whether an element is about to get cracked.

The process of crack propagation can be quantified by counting the number of elements with crack. As shown in Figure 11, the cracks propagate fast between the 1st and 4th second in the first heating pulse. Then it reaches saturation. The cracks have marginal propagation in the 1st cooling phase and the 2nd heating pulse, and then have absolutely no more propagation in the following heating pulse or cooling, since the number of cracked element is kept at 715. The peak crack length is kept at around 3mm. These numbers of cracked elements do not necessarily reflect the peak crack length.

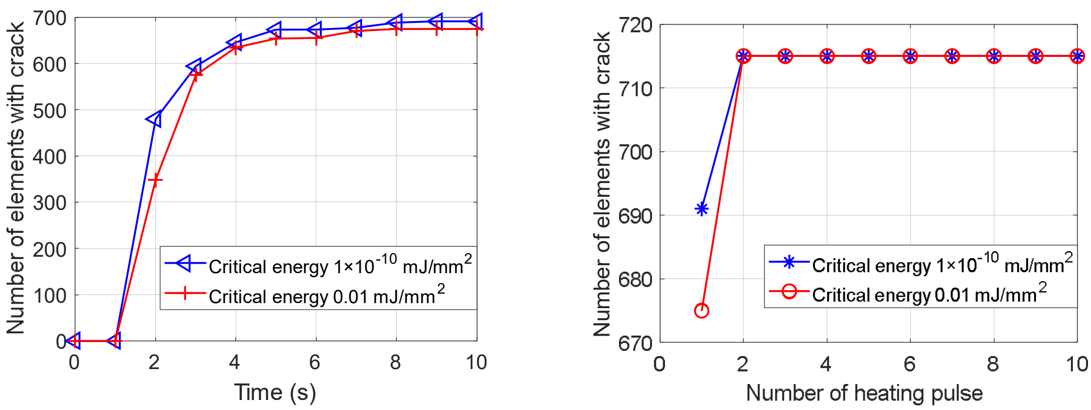

a) b)

Figure 11 Number of elements with crack, a) in the 1st heating pulse versus time, b) at the end of each heating pulse until 10th heating.

A further simulation has been performed with extreme conservative condition by setting critical energy to 1×10^{-10}mJ/mm^2, since zero is not acceptable in ABAQUS set up. The number of elements with cracks have also been collected in Figure 11.

Comparing the results with critical energy 0.01 and 1×10^{-10} mJ/mm^2, there is in between only marginal difference. After the end of 2nd heating pulse, the number of cracked elements are exactly the same for these two critical energies. Although in the 2nd until 10th heating pulse, the max. principal stress of the elements on the crack tip is still over the defined fracture strength (max. principal) 500MPa, and the critical energy is negligible, the cracks in these XFEM analyses have not propagated. This indicates that the calculated energy released rate near crack tip is close to zero, or is even negative when the crack tip is within a zone of compressive stress.

Two further XFEM simulations have been performed for linear elastic W by defining the fracture strength (max. principal strength) as 1000MPa, with critical energy 0.01 and 1×10^{-10} mJ/mm^2, respectively.

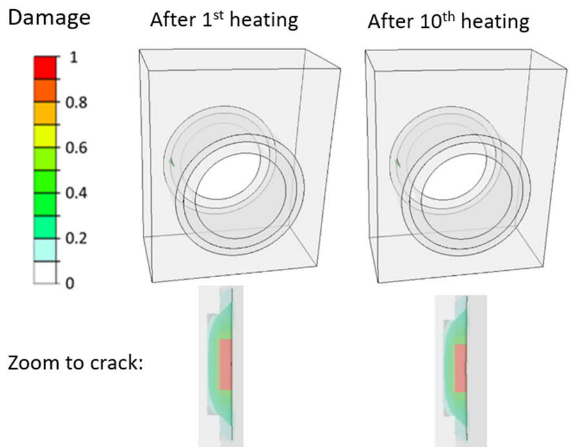

a) K_{ic} = 2 MPa · m$^{1/2}$ (Critical energy = 0.01 mJ/mm^2)

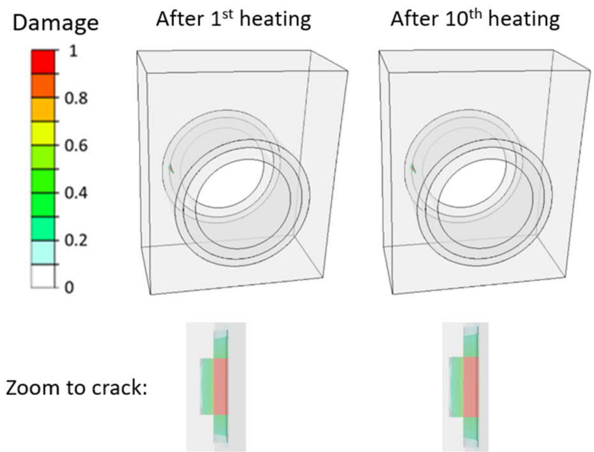

b) $K_{ic} = 2\times10^{-4}$ MPa · m$^{1/2}$ (Critical energy = 1×10^{-10} mJ/mm^2)

Figure 12 XFEM prediction of crack formation with heat flux 20MW/m^2, critical energy a) 0.01 mJ/mm^2 b) 1×10^{-10} mJ/mm^2, linear elastic W, fracture strength (max. principal strength) 1000MPa. The average element size in the W block close to W-Cu interface is $0.3\times0.3\times0.5$mm^3.

As similar to the cases with fracture strength 500MPa (Figure 10), the results for fracture strength

1000MPa (Figure 12) with two different critical energies have rare difference: the value of “status of XFEM” is different in only several elements on the crack tips, as shown in the “zoom to crack” in Figure 12.

The peak hoop stresses calculated for mesh size 0.3×0.3×0.5mm^3 in pure stress analysis is slightly over 1000MPa on both sides of angle ±75°, hence the crack only propagate inside several elements. As mentioned that the crack does not happen exactly simultaneously on the two sides, although the meshes and stresses are symmetric, the cracks for fracture strength 1000MPa (Figure 12) only happen on single side.

4.2 Simulation of cracks with material property changes for W

Based on the stress analysis in section 3.3 for those with material property changes during simulation, XFEM analyses for fracture has been performed for various heat fluxes.

As similar as the material-property-change process mentioned in section 3.3, the simulations start from pure stress calculation with elastic-ideal plastic W from the 1st to the 5th heating-cooling cycles, without XFEM analysis. Starting from the 6th cycle, the property of W-armor is set to be linear-elastic together with fracture strength and critical fracture energy, to start the XFEM analysis.

The purpose is to be closer to the actual working conditions where W-armor is exposed to irradiation and gradually loses its ductility. Due to the lack of material properties under real working conditions, a conservative assumption is made that irradiated tungsten has reduced the fracture toughness to a very low value, corresponding to enough large safety factor [16].

4.2.1 Heat flux 10 MW/m^2

With heat flux 10 MW/m^2, no crack is generated. According to the stress analysis in section 3.3 and the hoop stress distribution shown in Figure 8, the thermally induced stresses are less than 500MPa from the 6th to 10th heating-cooling cycles with heat flux 10 MW/m^2.

The plastic strain in W-armor is found to be zero if elastic-ideal plastic W is assumed.

4.2.2 Heat flux 15 MW/m^2

With heat flux 15 MW/m^2, cracks appear. XFEM analyses have been performed with various fracture toughness. The results have been collected in Table 4.

	K_{ic} = 2MPa·m$^{1/2}$	K_{ic} = 5MPa·m$^{1/2}$	K_{ic} = 10MPa·m$^{1/2}$	K_{ic} = 20MPa·m$^{1/2}$
Damage at the end of 6th heating 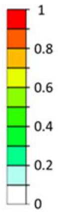	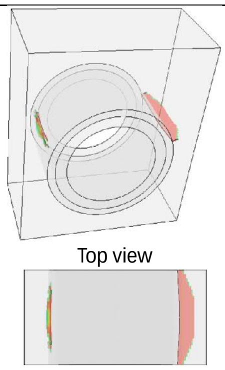	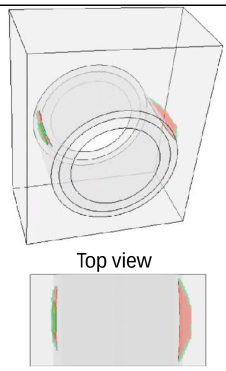	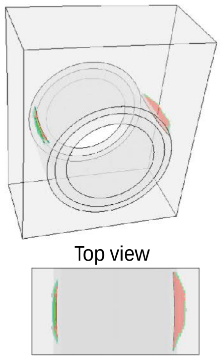	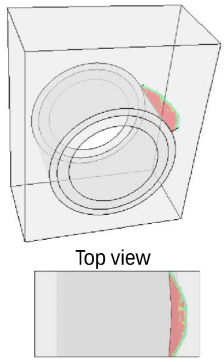
Damage at the end of 10th heating 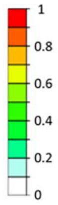	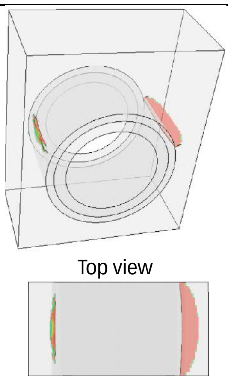	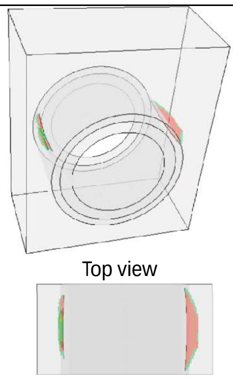	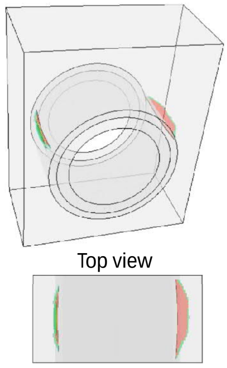	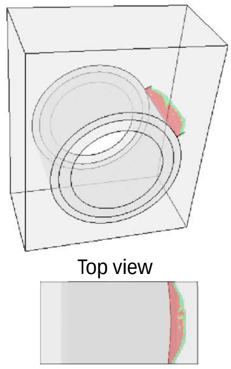

Table 4 XFEM prediction of crack formation with material property change for W-armor, heat flux 15MW/m^2, linear elastic W, fracture strength (max. principal strength) 500MPa. The average element size in the W block close to W-Cu interface is 0.3×0.3×0.5mm^3.

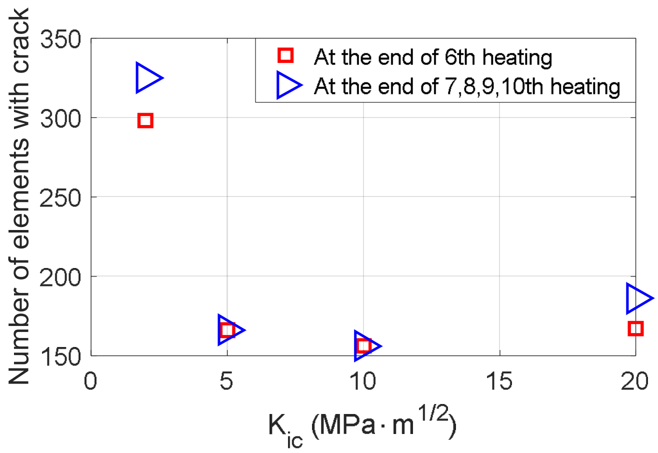

Figure 13 Number of elements with crack at the end of 6th and 10th heating pulse with different fracture toughness K_{ic}, 15MW/m^2

According to the stress analysis shown in Figure 8, the peak hoop stress is over 600MPa, hence cracks will appear if conservatively set the fracture strength to 500MPa [14].

As same as for linear elastic W (Figure 10, Figure 12), the cracks initiate and propagate in the first heating pulse when the XFEM analysis starts (6th heating pulse if material property change is included), as long as the calculated max. principal stress is higher than the defined critical value. Afterwards, there is rare or absolutely no more crack propagation in the following heating pulses or cooling.

As similar as Figure 11, the propagation of cracks is quantified by counting the number of cracked elements in the XFEM simulations, as collected in Figure 13. For K_{ic}= 2 & 20 MPa·$m^{1/2}$, the cracked elements have slightly increased from 6^{th} to 10^{th} heating pulses. And for K_{ic}= 5 & 10 MPa·$m^{1/2}$, there are absolutely no increase of cracked elements. The number of cracked elements doesn't necessarily reflect the peak crack length.

The asymmetry of crack initiation/propagation is obvious for these XFEM analyses with heat flux 15 MW/m^2 shown in Table 4. This asymmetry is till now unavoidable, since all different mesh configurations analyzed to date have displayed this asymmetric behavior, including various element sizes with various element shapes as brick, tetrahedron or triangular prism.

4.2.3 Heat flux 20 MW/m^2

XFEM analyses have been performed for heat flux 20MW/m^2 with various fracture toughness. The fracture strength is conservatively set to 500MPa for XFEM analysis. The results have been collected in Table 5.

	K_{ic} = 2MPa·$m^{1/2}$	K_{ic} = 10MPa·$m^{1/2}$	K_{ic} = 20MPa·$m^{1/2}$
Damage at the end of 6^{th} heating 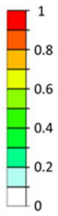	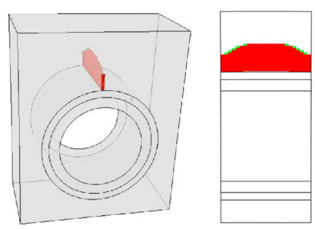	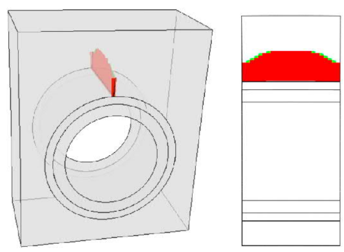	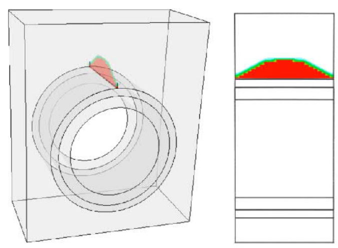
Damage at the end of 10^{th} heating 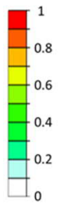	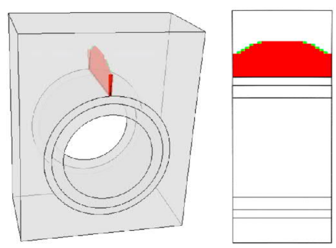	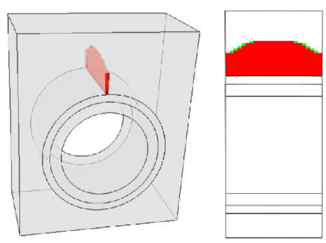	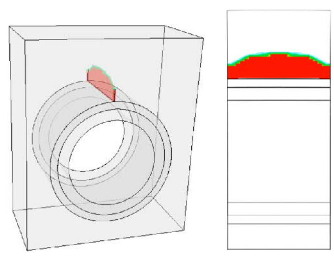

Table 5 XFEM prediction of crack formation with material property change for W-armor, heat flux 20MW/m^2, linear elastic W, fracture strength (max. principal strength) 500MPa. The average element size in the W block close to W-Cu interface is 0.4×0.4×0.5mm^3.

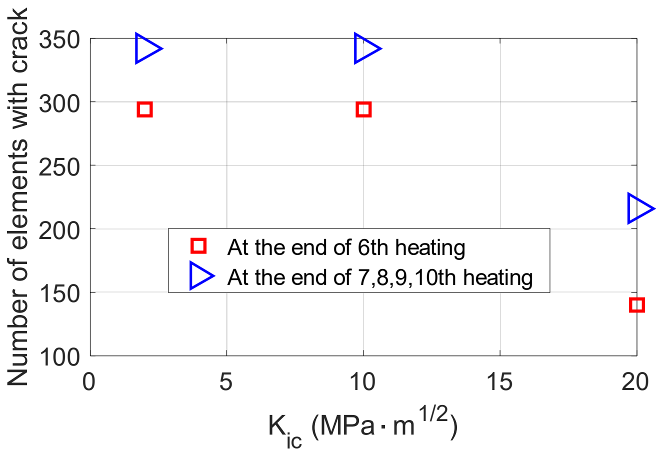

Figure 14 Number of elements with crack at the end of 6th and 10th heating pulse with different fracture toughness K_{ic}, 15MW/m^2

The numbers of cracked elements in the XFEM simulations have been collected in Figure 14 to quantify the propagation of cracks. The cracked elements have slightly increased from 6th to 10th heating pulses. And the influence of fracture toughness is marginal, since the number of cracked elements are the same for K_{ic}= 2 & 10 MPa·m$^{1/2}$. And this number for K_{ic}= 20 MPa·m$^{1/2}$ is slightly lower.

The crack initiates at the very top (angle zero) of the W-Cu interface with heat flux 20MW/m^2, while with heat flux 15MW/m^2, cracks initiate at two sides (angle around $\pm$75°). By checking the hoop stresses for both heat fluxes right before the crack initiation, it is clear that the XFEM-predicted cracks firstly appear at the locations where the calculated thermally induced stress firstly reaches the critical value. Note that in real component, the precondition for a crack initiation depends on more factors, including the distance to the nearest surface, and the type of loading (tensile-like or bending-type).

Concerning the different location of cracks for heat flux 15 and 20MW/m^2, as shown in Figure 15, with heat flux 15MW/m^2, the stress reaches the fracture strength 500MPa between time step 2.5~2.6s at angle around $\pm$75°; while with heat flux 20MW/m^2, the stress reaches 500MPa between time step 1.8~1.9s at angle zero.

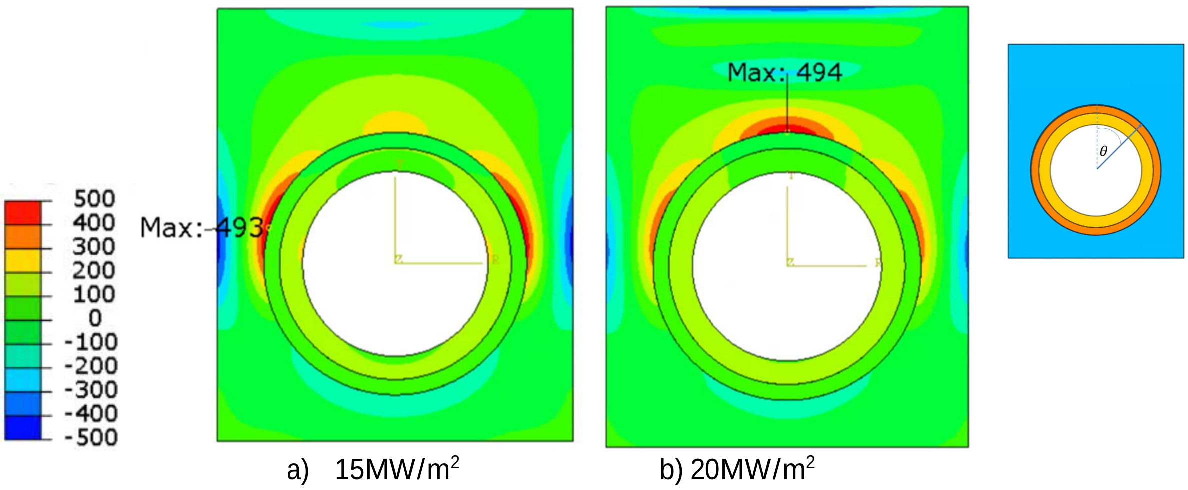

Figure 15 Hoop stresses distribution (in cylindrical coordinate system) on the plane of symmetry right before the crack initiation during the 6th heating pulse, with linear elastic-ideal plastic W in the 1st to 5th cycles . a) 15MW/m^2 at time step 2.5s b) 20MW/m^{2}at time step 1.8s. At the very next recorded time step (2.6s / 1.9s), cracks appear.

4.3 Issues in the XFEM analysis

One of the most critical issue with the XFEM analysis is that, the simulated cracks ceased further propagation after the first heating pulse, namely reaching a saturation. However, stress concentration along the crack tip has been detected as shown in *Figure 16* as an example, by setting critical energy to be 1×10^{-10}mJ/mm^2 as a negligible value. Further, the integrity has been already damaged by the crack generated during the first heating pulse.

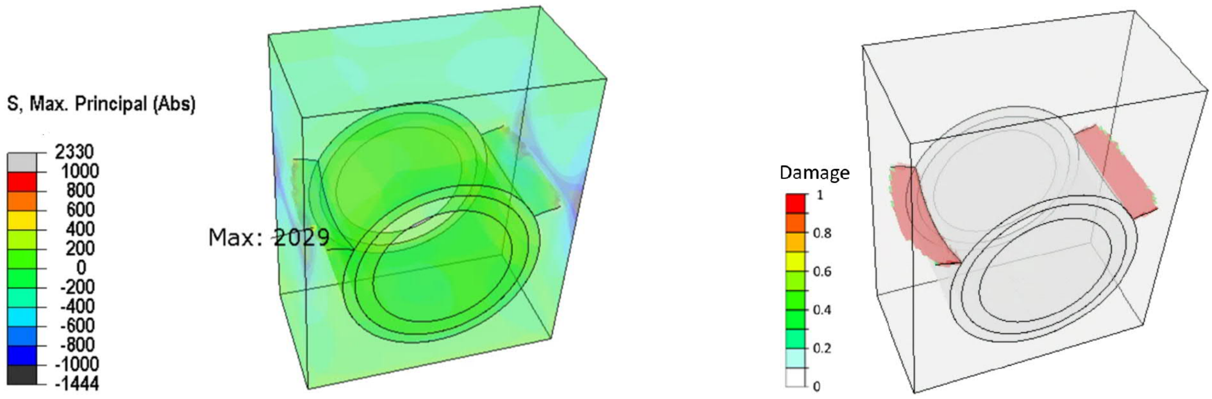

Figure 16 Stress profile (left) and XFEM prediction of crack formation (right) at the end of 10th heating pulse, heat flux 20MW/m^2, linear-elastic W. The average element size in the W block close to W-Cu interface is 0.4×0.4×0.5mm^3, assumed fracture strength 500MPa, critical energy set as 1×10^{-10}mJ/mm^2.

Further methods, such J-Integral calculation or stress analysis are necessary to verify these XFEM-predictions.

Another issue is the influence of mesh size on XFEM simulation.

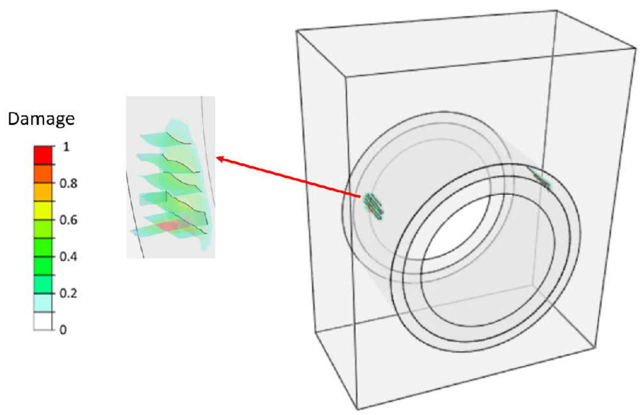

Figure 17 XFEM status at 1.076s in the first heating pulse, heat flux 20MW/m^2, linear-elastic W. The average element size in the W block close to W-Cu interface is 0.3×0.3×0.5mm^3, assumed fracture strength 500MPa, critical energy set as 0.01 mJ/mm^2.

In the XFEM simulation shown in Figure 17, finer mesh has been applied. The analysis stucks at time step 1.076s of the first heating pulse, right after the crack initiation. Comparing to the analysis presented in Figure 10 with mesh size 0.4×0.4×0.5mm^3, much more initial cracks appear. Since in XFEM analysis, once the stress is higher than the assumed critical value, crack initiates, and only one crack can initiate in one element. Hence, by using finer mesh, the thermally induced stress will reach the critical value simultaneously in more elements. These multi-initial-crack predicted by XFEM are actually related to real component, since under thermal-shock on perfect surfaces under symmetrical conditions, many micro-cracks initiate. In the course the density increases, until finally a few propagate further and all others are rested.

Another concern is raised due to the damage of heat flow within the tungsten armor due to the open cracks. Therefore, the heat flows have been checked. The heat flow profiles as well as temperature profiles of PFC under heat flux $20 MW/m^2$ at 1^{st}, 5^{th} and 10^{th} seconds in heating pulse have been collected in Figure 18.

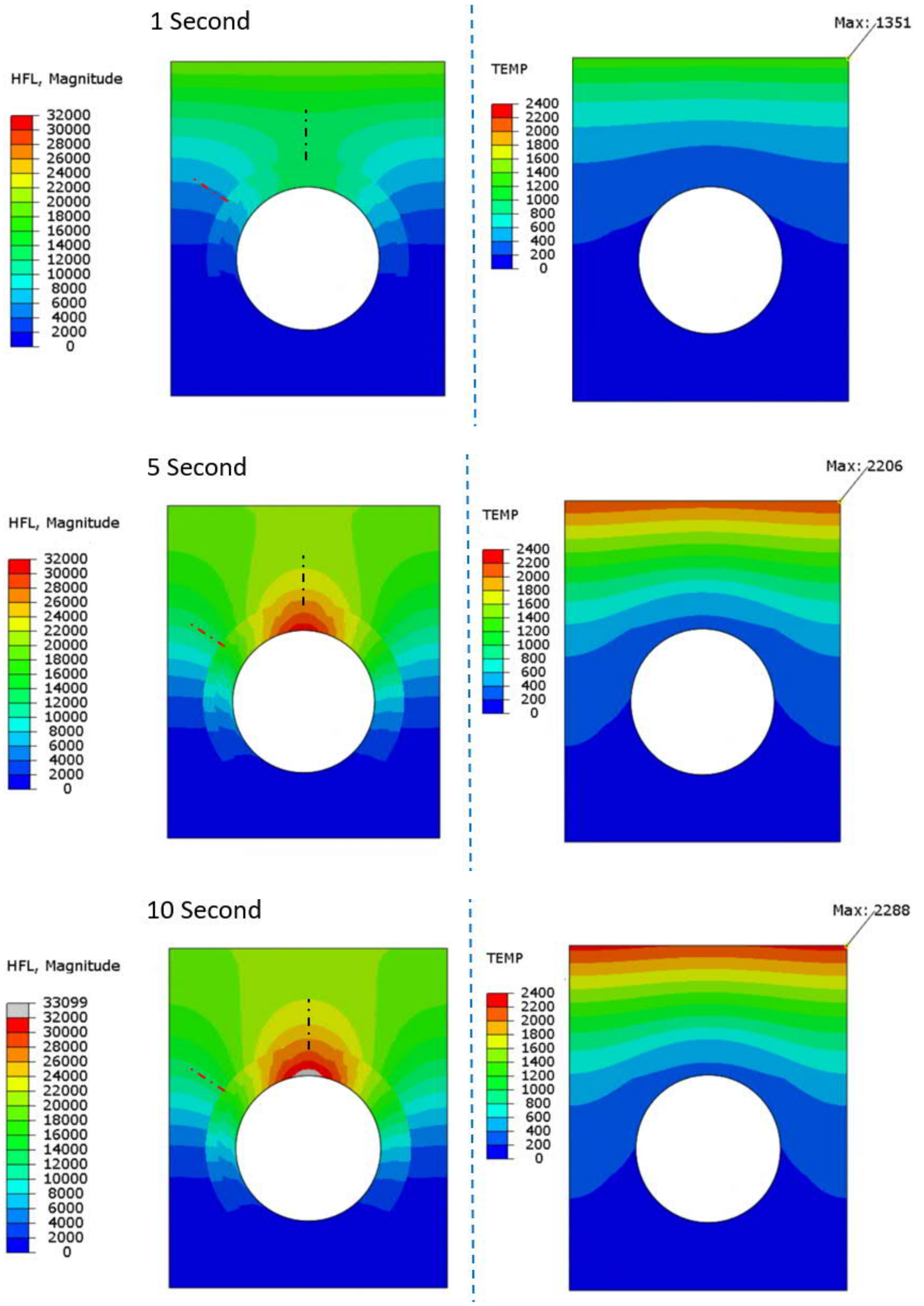

Figure 18 Heat flow within PFC & T-profile of PFC at 1st, 5th and 10th seconds during heating pulse, with heat flux 20MW/m^2. The position of angle 75° of one side is indicated by red dashed line. The position of angle 0° is indicated by black dashed line.

For the cracks occur on the top (angle 0°, marked in black), since the temperature distribution is symmetric, there is no temperature gradient, hence no heat flow across the crack.

For the cracks occur at the sides (angle ±75°, marked in red), the main paths of the heat flux flow is concentrated in the upper quarter region (between ±45°) of the W block. These lateral cracks are outside of this region, thus not hindering the main stream of the heat flow.

Another point is the critical heat flux (for the solid) occurs only under slow transients at 15-20MW/m^2 for around 10s. Under normal operation condition, the heat load (thus temperature) is so low that overheating of a cracked W block would not be an issue.

5. J-Integral calculation

Concerning the issue, whether cracks reaches saturation in the first heating pulse as XFEM-analysis suggested, static cracks with various lengths have been manually defined, instead of the cracks generated in XFEM-analysis, to calculate the J-Integral.

The manually defined crack is located on the side (angle 75°) with rectangular shape for simplicity through the thickness of 12mm, starting from the W-Cu interface, as shown in Figure 19.

The stress concentration around the crack tip is clear. J-Integrals at the crack tip have been calculated with 10 contours.

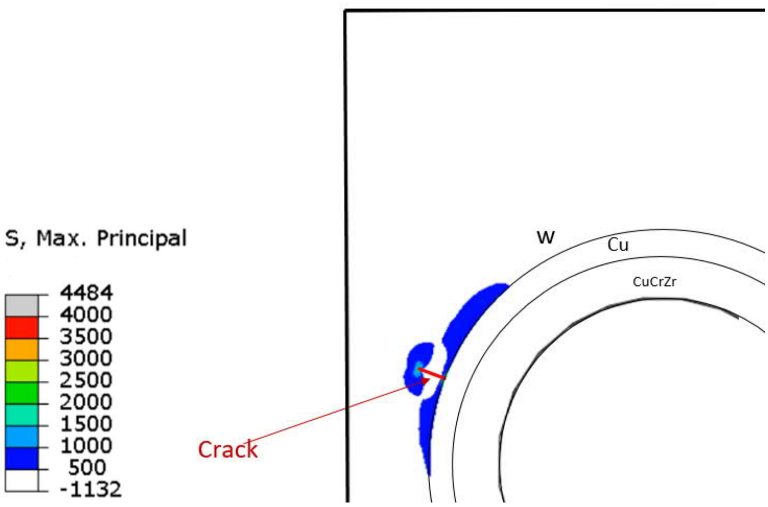

Figure 19 Manually defined static crack (1mm) to calculate J-Integral for various crack lengths. Max. principal stress over 500MPa is illustrated with colors. At the end of 1st heating pulse. Linear-elastic W. Heat flux 20MW/m^2.

As similar to the stress analysis in section 3 and fracture analysis in section 4, the mesh size and method have much influence on the calculated J-Integrals, especially the mesh of the elements around the crack tip.

In this work, meshes with various sizes and methods have been applied. It is found that, if the element shape is tetrahedron or triangular prism, the calculation will end up either with error or nonsensical results. Also, coarse mesh usually leads to too large calculated J-Integral.

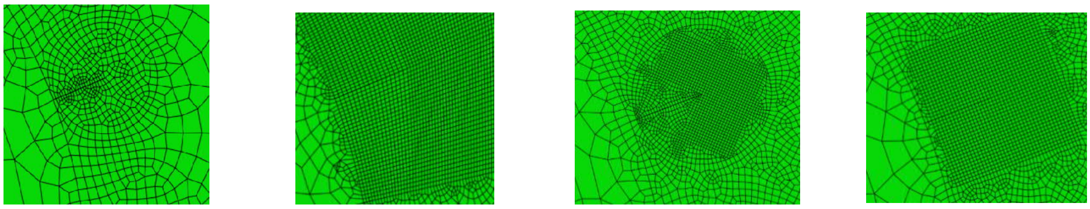

Mesh 1 Mesh 2 Mesh 3 Mesh 4

Figure 20 Four different mesh variants used for the calculation of J-Integral

By comparing the results with over 10 different meshes with various sizes and mesh types, several groups of results are comparable with each other. The meshes of these groups near the cracks have been shown in Figure 20. One group means a collection of J-Integrals for crack lengths ranging from 0.2mm to over 3mm with the same mesh size and method. The average length of the elements' edges around the crack tip are between 0.02mm and 0.06mm.

The J-Integral raises during the heating pulse and reaches its peak value at the end of the pulse, then decreases to negligible value during cooling phase, as one example shown in Figure 21.

These peak values of J-Integrals have been collected in Figure 22.

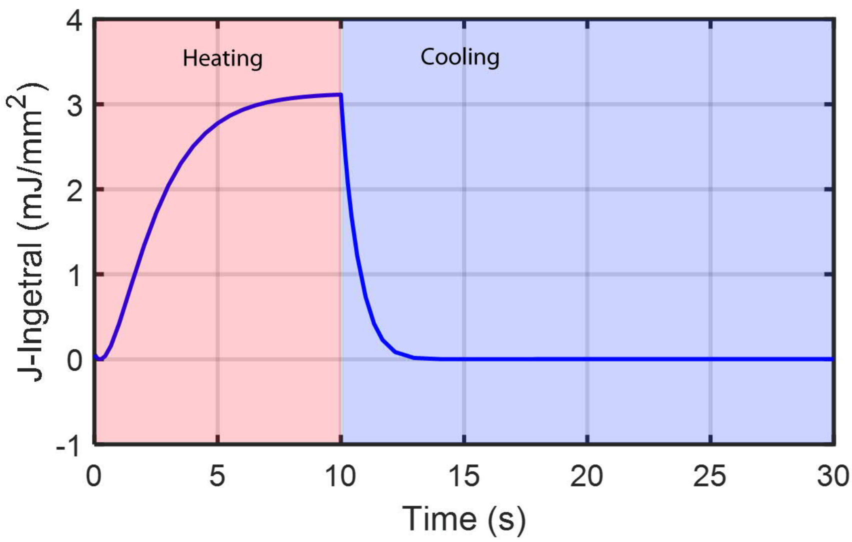

Figure 21 J-Integral vs. time, 1mm length crack with 20MW/m^2, linear-elastic W, mesh group 2.

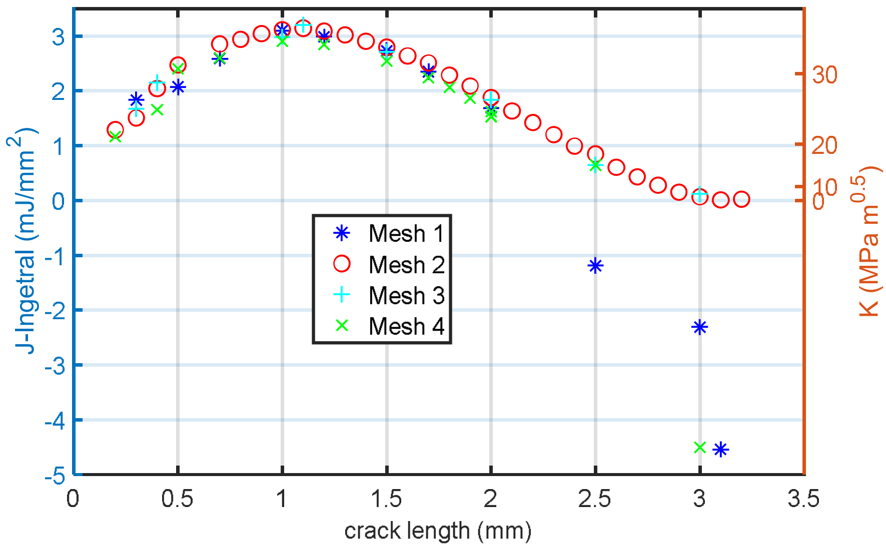

Figure 22 Collected J-Integral data calculated for the four meshing variants, with corresponding stress intensity factor (y-axis on the right).

The results in these four mesh groups (group 1-4) show that the J-Integrals increase when the crack lengths increase from 0.2mm to 1.1mm. The peak values are found at crack length 1.1mm. Then the J-Integrals decrease with the crack lengths increase further from 1.1mm to 3mm. Since the applied fracture toughness of tungsten is no more than 20MPa·m$^{1/2}$, no doubt that the crack will propagate in the first heating pulse.

According to the recent result of fracture toughness of irradiated tungsten [16] as shown in Figure 9, there have been rare data point over 20 MPa · m$^{1/2}$. However, corresponding stress intensity factor of the calculated J-Integral is already over 20 MPa · m$^{1/2}$ for crack length 0.2mm. Hence, it is very likely that, once the thermally induced stress is over the fracture strength, cracks will occur and propagate to at least 2.5mm.

Note that, if cracks initiate at the two sides (angle ±75°) as in Figure 19 and propagate along this angle, the maximum possible crack length is around 3.7mm until the component surface. The mesh is difficult if the manually defined crack is over 2.5mm, and the calculated J-Integral is mesh-dependent. The calculated J-Integrals of group 1 & 4 is negative for cracks over 2.5mm. In group 2 & 3, the calculated J-Integral tends to be zero if the crack length is over 3mm.

Further, the stress profiles have been checked. As shown in Figure 23, only elements of W with compressive stress are shown, while all elements with tensile stress have been hided.

It is clear that, there is a shell of compressive stress at the boundary of W-armor, where cracks should cease propagation.

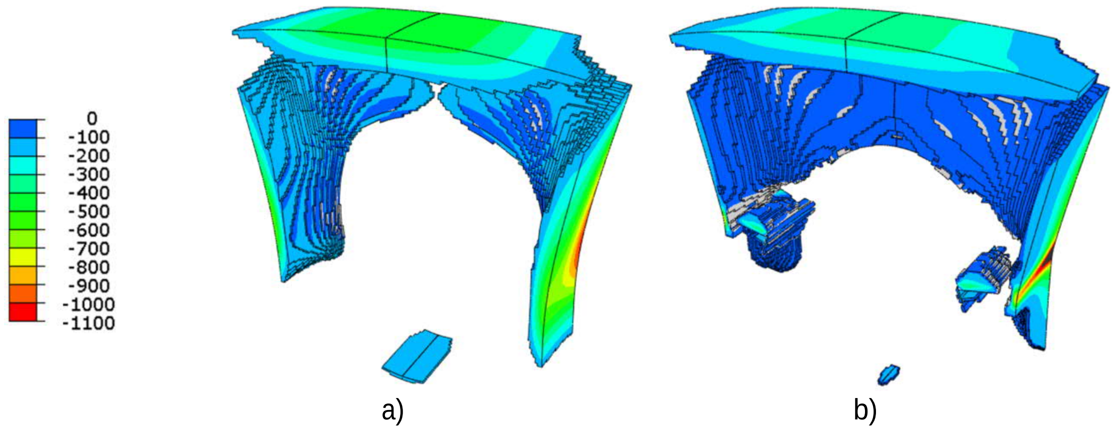

Figure 23 Region of compressive stress in the W monoblock. Minimum principal stress is plotted. Linear-elastic W, average length of element's edge is 0.1mm, at the end of first heating pulse, with heat flux 20MW/m^2. a) No crack b) 3mm crack

Hence, this shell of compressive stress well explains the issue raised in XFEM analysis in section 4.3, since cracks will cease to propagate in a zone with compressive stress. Also, this shell explains that there are several negative J-Integral values with crack length over 2.5mm (Figure 22).

Therefore, in these three groups of analyses,

1. XFEM-simulation,
2. J-Ingetral calculation
3. stress analysis shown in Figure 23,

all of them have predicted that the crack will cease propagation after it reach a length of around 3mm.

6. Conclusion

A series of FEM simulations have been performed for the design of divertor for European DEMO. The capability of FEM simulation and issues raised in the FEM simulations have been discussed. Several key findings are as follows:

1. Crack initiation was predicted only when a hypothetically low tensile strength (half the measured actual value) was assumed.
2. The predicted location of cracking was affected by the material models (elastic vs. plastic) assumed for the simulation.
3. XFEM simulation predicted that even such hypothetical cracks did not grow already after the first loading pulse.
4. The cracking pattern and extent predicted by the XFEM simulation agreed well with the results of J-integral calculation conducted for the same pre-crack location as a function of crack size.
5. An envelope region of compressive stress field surrounding the cracks in the tungsten armour block under heat loads explains the early saturation of crack growth.

This work follows the concept of “design-by-analysis” [4] with conservative assumptions of plasticity, fracture strength and fracture toughness. Dedicated experiments are required in the future for the verification of FEM analysis.

Acknowledgement

This work has been carried out within the framework of the EUROfusion Consortium and has received funding from the Euratom research and training programme 2014-2018 and 2019-2020 under grant agreement No 633053. The views and opinions expressed herein do not necessarily reflect those of the European Commission.

References

[1] J.-H. You, "A review on two previous divertor target concepts for DEMO: mutual impact between structural design requirements and materials performance," Nuclear Fusion, vol. 55, no. 113026, 2015.

[2] F. Romanelli, "Fusion electricity-a roadmap to the realization of fusion energy," European Fusion Development Agreement, ISBN 978-3-00-040720, 2012.

[3] A. Donné, "Roadmap Towards Fusion Electricity (Editorial).," J Fusion Energ, pp. 503-505, 2019.

[4] J.-H. You, M. Li and K. Zhang, "Structural lifetime assessment for the DEMO- divertor targets: Design-by-analysis approach and outstanding issues," Fusion Engineering and Design, vol. 164, no. 112203, March 2021.

[5] M. Li, F. Gallay, M. Richou and J.-H. You, "Fracture mechanical analysis of a tungsten monoblock-type plasma-facing component without macroscopic interlayer for high-heat-flux divertor target," Fusion Engineering and Design, vol. 122, pp. 124-130, 2017.

[6] M. Li and J.-H. You, "Structural impact of creep in tungsten monoblock divertor target at 20 MW/m2," Nuclear Materials and Energy, vol. 14, pp. 1-7, 2018.

[7] E. Sieder and G. Tate, "Heat transfer and pressure drop of liquids in tubes," Industrial & Engineering Chemistry Research, vol. 28, pp. 1429-1435, 1936.

[8] J. Thom, W. Walker, T. Fallon and G. Reising, "Boiling in sub-cooled water during flow up heated tubes or annuli," Proceedings of the Institution of Mechanical Engineers, vol. 180, pp. 226-246, 1965-1966.

[9] E. Visca, E. Cacciotti, A. Komarov, S. Libera, N. Litunovsky, A. Makhankov, A. Mancini, M. Merola, A. Pizzuto, B. Riccardi and S. Roccella, "Manufacturing, testing and post-test examination of ITER divertor vertical target W small scale mock-ups," Fusion Engineering and Design, vol. 86, p. 1591–1594, 2011.

[10] ITER structural design criteria for in-vessel components (SDC-IC), "Appendix A: Materials design limit data," ITER, 2012.

[11] ITER Document No.G74 M 16, "ITER Material Properties Handbook," 2005.

[12] K. Zhang, E. Gaganidze and M. Gorley, "Development of the material property handbook and database of CuCrZr," Fusion Engineering and Design, vol. 144, pp. 148-153, 2019.

[13] E.Gaganidze, A.Chauhan, H.-C.Schneider, D.Terentyev, G.Borghmans and J.Aktaa, "Fracture-mechanical properties of neutron irradiated ITER specification tungsten," Journal of Nuclear Materials, vol. 547, no. 152761, 15 April 2021.

[14] C. Yin, D. Terentyev, T. Zhang, R. H.Petrov and T. Pardoen, "Impact of neutron irradiation on the

strength and ductility of pure and ZrC reinforced tungsten grades," Journal of Nuclear Materials, vol. 537, 2020.

[15] "The extended finite element method (XFEM)," [Online]. Available: https://abaqus-docs.mit.edu/2017/English/SIMACAECAERefMap/simacae-c-engconcxfemoverview.htm.

[16] E. Gaganidze, A. Chauhan, H.-C. Schneider, D. Terentyev, B. Rossaert and J. Aktaa, "Effect of irradiation temperature on the fracture-mechanical behaviour of tungsten irradiated to 1 dpa," Journal of Nuclear Materials, vol. 556, no. 153200, 2021.